Simplified Syndrome-based Decoding of Punctured Convolutional Codes

Jérémy Nadal, Joseph Jabour, Stefan Weithoffer, Charbel Abdel Nour, Catherine Douillard

▶ **To cite this version:**

Jérémy Nadal, Joseph Jabour, Stefan Weithoffer, Charbel Abdel Nour, Catherine Douillard. Simplified Syndrome-based Decoding of Punctured Convolutional Codes. ISTC 2025: International Symposium on Topics in Coding, Aug 2025, Los angeles, CA, United States. pp.1-5, ⟨10.1109/ISTC65386.2025.11154626⟩. ⟨hal-05168400⟩

HAL Id: hal-05168400

https://imt-atlantique.hal.science/hal-05168400v1

Submitted on 17 Jul 2025

HAL is a multi-disciplinary open access archive for the deposit and dissemination of scientific research documents, whether they are published or not. The documents may come from teaching and research institutions in France or abroad, or from public or private research centers.

L'archive ouverte pluridisciplinaire **HAL**, est destinée au dépôt et à la diffusion de documents scientifiques de niveau recherche, publiés ou non, émanant des établissements d'enseignement et de recherche français ou étrangers, des laboratoires publics ou privés.

HAL Authorization

Simplified Syndrome-based Decoding of Punctured Convolutional Codes

Jeremy Nadal, Joseph Jabour, Stefan Weithoffer, Charbel Abdel Nour, Catherine Douillard
IMT Atlantique, Lab-STICC, UMR CNRS 6285, F-29238 Brest, France

***Abstract*—This paper introduces a convolutional syndrome former (CSF) which enables reduced complexity decoding of regularly punctured convolutional codes (CCs) of rate $r/(r+1)$. The CSF is derived by reformulating the parity-check constraints using the punctured dual codewords, and can be implemented either as a parity-check matrix (PCM) or as a multi-binary convolutional (MBC) structure. The former approach significantly reduces the complexity of the decoding process compared to conventional maximum a posteriori (MAP) decoding. Simulation results show that belief propagation (BP) decoding on the CSF achieves comparable performance to conventional MAP decoding, with a penalty of only 0.1 dB. Additionally MAP decoding on the MBC trellis yields identical performance. This enables a decoding complexity reduction ranging from 50% to 90% depending on the code rate. Furthermore, simulation results for turbo decoding shows around 0.3 dB degradation at lower rates and minimal impact (less than 0.15 dB) at higher rates compared to iterative MAP-based decoding.**

***Index Terms*—Convolutional codes, Low complexity decoding**

I. Introduction

Convolutional codes (CCs) are a well-established class of error-correcting codes knwon for their flexible code rates and efficient encoding, while maintaining relatively low decoding complexity. These attributes have made them invaluable in applications such as 4G control channels [1] and systems with constrained receiver hardware. However, efficient decoding of high-rate CCs remains challenging, particularly for high-throughput applications that typically operate at high coding rates. The complexity of maximum a posteriori (MAP) decoding is dictated by the underlying base code rather than the punctured code, making it essential to simplify the decoding process for high-rate CCs. This is not only crucial for CC decoding but also for concatenated codes and especially turbo codes (TCs), which rely on their constituent CCs [2].

In this work, we introduce a novel *convolutional syndrome former (CSF)* representation that captures the relationship between parity and systematic bits in regularly punctured CCs with a rate of $r/(r+1)$. The CSF is derived by leveraging and reformulating a specifically designed dual code for the punctured CC. Decoding using the CSF can be implemented in several ways, including as a multi-binary convolutional (MBC) structure. Additionally, since the CSF is inherently a parity-check matrix (PCM), it lends itself to the application of belief propagation (BP), significantly reducing decoding complexity. This approach extends to turbo codes (TCs), thereby reducing the decoding complexity for both punctured CCs and TCs.

The paper is structured as follows: section II provides the necessary background on CCs, encoding, termination, and puncturing. Section III details the proposed CSF structure for regularly punctured CCs. Section IV discusses maximum a posteriori (MAP)-based and BP-based decoding approaches, including their respective complexities. Section V explores the application to TCs. Finally, section VI concludes the paper.

II. Convolutional Codes

A rate-1/2 recursive systematic CC is characterized by its recursive polynomial $\boldsymbol{g}_r$ and its parity polynomial $\boldsymbol{g}_p$, both of length-$(\nu+1)$ with ν being the number of memory elements (MEs). Given an input sequence $\boldsymbol{x}$ of K bits, the encoder produces a codeword (CW) $\boldsymbol{c}$ of $2K$ bits. The code being systematic, the CW $\boldsymbol{c}$ is formed by the concatenation of the original input sequence $\boldsymbol{x}$ and the corresponding parity sequence $\boldsymbol{y}$, i.e., $\boldsymbol{c}=[\boldsymbol{x},\boldsymbol{y}]$. At time instance $t \in [\![0, K-1]\!]$ of the encoding process, a recursive bit $\boldsymbol{r}[t]$ and a parity bit $\boldsymbol{y}[t]$ are generated following

$$\boldsymbol{r}[t] = \mathbf{g}_r \times [\boldsymbol{x}[t], \boldsymbol{s}_t]^\dagger, \quad \boldsymbol{y}[t] = \mathbf{g}_p \times [\boldsymbol{r}[t], \boldsymbol{s}_t]^\dagger, \qquad (1)$$

where $\dagger$ is the transpose operator and the state vector of the ν MEs at instance t is represented by $\boldsymbol{s}_t$. All mathematical operations are defined in Galois Field GF(2). Tail-biting (TB) termination [3] is adopted since other termination schemes can be seen as an instance of TB.

Puncturing is applied to achieve higher coding rates by selectively omitting some encoded bits before transmission. The puncturing is commonly performed on the parity bits $\boldsymbol{y}$ by a transmission mask $\boldsymbol{m}$ of size M which includes the indices of the transmitted parity bits, $\boldsymbol{z}$, such that[1] $\boldsymbol{z}=\boldsymbol{y}[\boldsymbol{m}]$.

After puncturing, the CW $\tilde{\boldsymbol{c}}=[\boldsymbol{x},\boldsymbol{z}]$ is formed with a resulting code rate of $R=K/(K+M)$. The major drawback of the puncturing approach is that the decoding complexity remains dictated by the underlying unpunctured base code. Therefore, an alternative representation of the punctured CCs is derived in the following section. This representation is based on the reformulation of parity constraints that relate the information and redundancy bits, enabling low-complexity decoding of rate $R_r \triangleq r/(r+1)$ regularly punctured CCs, where r is the puncturing pattern period. Note, that we consider in the following a regular transmission mask $\boldsymbol{m}$ expressed as

$$\boldsymbol{m}[j] = rj + \Gamma \qquad (2)$$

with an offset position $\Gamma \in [\![0, r-1]\!]$.

[1]To ease derivations, indexing in form of vector is allowed: $\tilde{\boldsymbol{x}}=\boldsymbol{x}[\boldsymbol{m}] \Leftrightarrow \tilde{\boldsymbol{x}}[i]=\boldsymbol{x}[\boldsymbol{m}[i]]$ and $\tilde{\boldsymbol{X}}=\boldsymbol{X}[\boldsymbol{m},-] \Leftrightarrow \tilde{\boldsymbol{X}}[i,j]=\boldsymbol{X}[\boldsymbol{m}[i],j]$.

III. Proposed Convolutional Syndrome Former

The essence of the proposed framework is to determine a suitable CSF matrix $\boldsymbol{F}$, which, when applied to a CW generated by the original punctured CC, yields an all-zero output, i.e., $\tilde{\boldsymbol{c}}\boldsymbol{F} = \boldsymbol{0}$. This section presents a method for constructing the CSF matrix as follows:

1) Find a suitable dual of the $1/2$-rate RSC encoder;
2) Find a constrained dual return-to-zero (RTZ) sequence;
3) Encode M rotated sequences via the dual encoder;
4) Concatenate punctured dual CWs to form a CSF matrix.

The choices in steps 1) and 2) are designed to ensure that the CSF matrix exhibits a repetitive (convolutional) structure with a low density of non-zero values, by applying the duality property to sub-codewords. This results in a CSF that can be effectively utilized for decoding either through its Tanner graph representation (section III-C) or as an MBC structure (section III-D).

A. Dual Convolutional Code

The dual code of a linear code $\mathcal{C}$ with rate K/N, $\mathcal{C}^{\perp}$, is a linear code of rate $(N-K)/N$ whose CWs are orthogonal to the CWs of $\mathcal{C}$. A generator matrix of $\mathcal{C}^{\perp}$ is a parity matrix of $\mathcal{C}$: $\boldsymbol{G}_{\perp} = \boldsymbol{H}$. Hence, in the base domain, K bits are encoded to output $K+M$ bits and in the dual domain, M bits are encoded to output $K+M$.

Lemma III.1. *Reversing the bit-order (with elements denoted by $\overleftarrow{\cdot}$) of the TB-CC polynomials $(\boldsymbol{g}_r, \boldsymbol{g}_p)$ yields a dual code representation with generator matrix $\boldsymbol{G}_{\perp} = \left[\boldsymbol{G}_{\overleftarrow{\boldsymbol{r}}}^{-1}\boldsymbol{G}_{\overleftarrow{\boldsymbol{p}}}, \boldsymbol{I}_K\right]$, derived from $\overleftarrow{\boldsymbol{g}_r}$ and $\overleftarrow{\boldsymbol{g}_p}$ with*

$$\overleftarrow{\boldsymbol{g}_x}[i] \triangleq \boldsymbol{g}_x[mod_{\nu}(-i-1)], \quad i \in [\![0, \nu]\!].$$

Proof. Let $\boldsymbol{G} = [\boldsymbol{G_r}, \boldsymbol{G_p}]$ be a generator matrix of size $K \times 2K$, corresponding to a rate-$1/2$ TB-CC with polynomials $\boldsymbol{g}_r$ and $\boldsymbol{g}_p$. For a valid dual code, $\boldsymbol{G}_{\perp}\boldsymbol{G}^{\dagger} = \boldsymbol{0} \Leftrightarrow \boldsymbol{G}_{\overleftarrow{\boldsymbol{r}}}\boldsymbol{G}_{\perp}\boldsymbol{G}^{\dagger} = \boldsymbol{0}$. Thus,

$$\boldsymbol{G}_{\overleftarrow{\boldsymbol{r}}}\boldsymbol{G}_{\perp}\boldsymbol{G}^{\dagger} = [\boldsymbol{G}_{\overleftarrow{\boldsymbol{p}}}, \boldsymbol{G}_{\overleftarrow{\boldsymbol{r}}}][\boldsymbol{G_r}, \boldsymbol{G_p}]^{\dagger} = \boldsymbol{G}_{\overleftarrow{\boldsymbol{p}}}\boldsymbol{G}_{\boldsymbol{r}}^{\dagger} + \boldsymbol{G}_{\overleftarrow{\boldsymbol{r}}}\boldsymbol{G}_{\boldsymbol{p}}^{\dagger}.$$

The matrices $\boldsymbol{G}$ and $\boldsymbol{G}_{\perp}^{\dagger}$ are circulant. The transpose of a circulant matrix $\boldsymbol{G}_x$, $\boldsymbol{G}_x^{\dagger}$, can be expressed as[2]

$$\boldsymbol{G}_x^{\dagger} = \underset{-\nu}{\circlearrowleft}(\boldsymbol{G}_{\overleftarrow{x}}) = \underset{-\nu}{\circlearrowleft}(\boldsymbol{I}_K)\boldsymbol{G}_{\overleftarrow{x}} \Leftrightarrow \boldsymbol{G}_{\overleftarrow{x}} = \underset{\nu}{\circlearrowleft}(\boldsymbol{I}_K)\boldsymbol{G}_x^{\dagger}, \quad (3)$$

where $\boldsymbol{I}_K$ is the size-K identity matrix. The product of the circulant matrices is commutative. Thus,

$$\boldsymbol{G}_{\overleftarrow{\boldsymbol{r}}}\boldsymbol{G}_{\perp}^{\dagger}\boldsymbol{G} = \boldsymbol{G}_{\boldsymbol{p}}^{\dagger}\underset{\nu}{\circlearrowleft}(\boldsymbol{I}_K)\underset{-\nu}{\circlearrowleft}(\boldsymbol{I}_K)\boldsymbol{G}_{\overleftarrow{\boldsymbol{r}}} + \boldsymbol{G}_{\overleftarrow{\boldsymbol{r}}}\boldsymbol{G}_{\boldsymbol{p}}^{\dagger} = \boldsymbol{0}. \quad \square$$

Deriving the dual code using bit reversal of the base polynomials, which produces dual CWs of the form $\boldsymbol{c}^{\perp} = [\boldsymbol{y}^{\perp}, \boldsymbol{x}^{\perp}]$, offers two advantages: First, the dual systematic sequence $\boldsymbol{x}^{\perp}$ occupies the same position as the parity sequence $\boldsymbol{y}$ in the base CW $\boldsymbol{c} = [\boldsymbol{x}, \boldsymbol{y}]$, and the dual parity sequence $\boldsymbol{y}^{\perp}$ aligns with the systematic sequence $\boldsymbol{x}$. Second, reversing the polynomials preserves the CC structure, simplifying the search for low-weight dual CWs.

[2]Operator $\underset{r}{\circlearrowleft}$ performs a right rotation by r positions if $r > 0$ (left rotation if $r < 0$) on the elements of a vector $\boldsymbol{x}$ or the columns of a matrix $\boldsymbol{X}$

B. Generation of a Convolutional Syndrome Former

1) Search for a constrained dual RTZ sequence: This step requires identifying a constrained dual RTZ sequence $\boldsymbol{x}^{\perp}$ of length K that is an RTZ sequence [4] of the dual encoder derived in Sect. III-A, has bits equal to 0 at positions corresponding to the puncturing mask $\overline{\boldsymbol{m}}$: $\boldsymbol{x}^{\perp}[\overline{\boldsymbol{m}}] = \boldsymbol{0}$, and satisfies $\boldsymbol{x}^{\perp}[\Gamma] = 1$. The search for $\boldsymbol{x}^{\perp}$ can be performed exhaustively over a limited number of non-zero positions in $\boldsymbol{x}^{\perp}$, or based on the reduction function from [4].

2) Encoding M circularly shifted versions of $\boldsymbol{x}^{\perp}$: The CSF structure must account for constraints related to all M non-punctured positions defined by $\boldsymbol{m}$. Hence, M distinct dual input sequences $\boldsymbol{x}_i^{\perp}$, $i \in [\![0, M-1]\!]$, are required, each satisfying the RTZ property mentioned in Section III-B1. Given the assumed regularity (with period r) of the non-punctured positions $\boldsymbol{m}$, the M input sequences $\boldsymbol{x}_i^{\perp}$ are obtained by circularly shifting the base sequence $\boldsymbol{x}^{\perp}$ identified previously:

$$\boldsymbol{x}_i^{\perp} = \underset{ir}{\circlearrowleft}(\boldsymbol{x}^{\perp}), \quad i \in [\![0, M-1]\!]. \quad (4)$$

Each vector $\boldsymbol{x}_i^{\perp}$ is then encoded using the dual TB-CC encoder, defined by its generator matrix $\boldsymbol{G}_{\perp}$. This encoding produces M dual parity sequences $\boldsymbol{y}_i^{\perp}$ and corresponding dual CWs $\boldsymbol{c}_i^{\perp} = \boldsymbol{x}_i^{\perp}\boldsymbol{G}_{\perp} = \left[\boldsymbol{y}_i^{\perp}, \boldsymbol{x}_i^{\perp}\right]$.

3) Concatenation of the punctured dual CWs: With the dual code representation adopted in Section III-A, puncturing the parity bits of an original TB-CC CW $\boldsymbol{c}$ corresponds to puncturing the systematic part of the dual CW $\boldsymbol{c}^{\perp}$. Thus, the punctured dual CWs $\tilde{\boldsymbol{c}}_i^{\perp}$ are formed by retaining the dual parity part $\boldsymbol{y}_i^{\perp}$ and the bits of the dual systematic part $\boldsymbol{x}_i^{\perp}$ that align with the non-punctured positions $\boldsymbol{m}$, resulting in $\tilde{\boldsymbol{c}}_i^{\perp} = \left[\boldsymbol{y}_i^{\perp}, \boldsymbol{z}_i^{\perp}\right]$, where $\boldsymbol{z}_i^{\perp}[j] = \boldsymbol{x}_i^{\perp}[\boldsymbol{m}]$. The CSF $\boldsymbol{F}$ is then derived according to (5):

Lemma III.2. *The concatenation of punctured dual CWs $\tilde{\boldsymbol{c}}_i^{\perp}$ results in a CSF matrix $\boldsymbol{F}$ given by*

$$\boldsymbol{F} = \left[(\tilde{\boldsymbol{c}}_i^{\perp})^{\dagger}\right]_{i \in [\![0, M-1]\!]}. \quad (5)$$

Proof. Given a rate-$1/2$ CC code with PCM $\boldsymbol{H}_{\text{base}}$ composed of two $K \times K$ circulant matrices $\boldsymbol{H}_{\text{base}} = [\boldsymbol{Y}^{\perp}, \boldsymbol{X}^{\perp}]$, it is shown in [5][3] that a size-$(M \times N)$ PCM $\boldsymbol{H} = \boldsymbol{F}^{\dagger}$ of the punctured TB-CC code with transmission mask $\boldsymbol{m}$ (M parity bits) is $\boldsymbol{H} = \left[\boldsymbol{Y}^{\perp}[\boldsymbol{m}, -], \boldsymbol{X}^{\perp}[\boldsymbol{m}, \boldsymbol{m}]\right]$ if and only if $\boldsymbol{X}^{\perp}$ satisfies:

$$\boldsymbol{X}^{\perp}[\boldsymbol{m}, \overline{\boldsymbol{m}}] = \left(\boldsymbol{X}^{\perp}[\overline{\boldsymbol{m}}, \boldsymbol{m}]\right)^{\dagger} = \boldsymbol{0}, \quad (6)$$

with $\overline{\boldsymbol{m}}$ being the puncturing mask ($K-M$ punctured bits). Recall that $\boldsymbol{x}^{\perp}[\overline{\boldsymbol{m}}] = \boldsymbol{0}$ for the constrained dual RTZ sequence defined in Section III-B1. Let $\boldsymbol{X}^{\perp} = \left[(\boldsymbol{x}_l^{\perp})^{\dagger}\right]_{l \in [\![0, K-1]\!]}^{\dagger}$ with K rows, each row being composed of $\boldsymbol{x}^{\perp}$ shifted by $l - \Gamma$: $\boldsymbol{x}_l^{\perp} = \circlearrowleft_{l-\Gamma}(\boldsymbol{x}^{\perp})$. Since $\circlearrowleft_i(\boldsymbol{x})[\boldsymbol{m}] = \boldsymbol{x}[\boldsymbol{m} - i]$, we have

$$\boldsymbol{X}^{\perp}[\boldsymbol{m}[i], \overline{\boldsymbol{m}}] = \underset{ir}{\circlearrowleft}(\boldsymbol{x}^{\perp})[\overline{\boldsymbol{m}}] = \boldsymbol{x}^{\perp}[\overline{\boldsymbol{m}} - ir] = \boldsymbol{0}, \forall i. \quad (7)$$

[3]In [5], $(\boldsymbol{X}^{\perp}, \boldsymbol{Y}^{\perp})$ are denoted $(\boldsymbol{T}, \boldsymbol{G})$ in eq. (8) and (11).

Therefore, $\boldsymbol{X}^{\perp}[\boldsymbol{m}, \overline{\boldsymbol{m}}] = \mathbf{0}$. To prove $\left(\boldsymbol{X}^{\perp}[\overline{\boldsymbol{m}}, \boldsymbol{m}]\right)^{\dagger} = \mathbf{0} \Leftrightarrow \left(\boldsymbol{X}^{\perp}\right)^{\dagger}[\boldsymbol{m}, \overline{\boldsymbol{m}}] = \mathbf{0}$, we start from the observation that $\boldsymbol{x}_0^{\perp}$ can always be decomposed into a length-L_v sequence $\boldsymbol{v}$ followed by $K - L_v$ zeros, $\boldsymbol{x}_0^{\perp} = [\boldsymbol{v}, \mathbf{0}]$, s. t. $\exists k, L_v = kr+1$. Moreover, $\boldsymbol{v}[i] = \overleftarrow{\boldsymbol{v}}[i] = 0$ if $\mathrm{mod}_r(i) \neq 0$. Applying (3), we obtain:

$$\left(\boldsymbol{X}^{\perp}\right)^{\dagger}[\boldsymbol{m}[i], \overline{\boldsymbol{m}}] = \underset{r(i-k)}{\circlearrowleft}([\overleftarrow{\boldsymbol{v}}, \mathbf{0}])[\overline{\boldsymbol{m}}] = \mathbf{0}, \forall (i,k). \quad \square$$

C. Deriving a Tanner Graph from the CSF Matrix

The CSF matrix $\boldsymbol{F} = \boldsymbol{H}^{\dagger}$ can be represented using a Tanner graph with M check nodes (CNs) and N variable nodes (VNs), enabling BP decoding. To significantly reduce or eliminate the girth-4 cycles degrading BP performance, we introduce M auxiliary VNs [6], yielding an expanded CSF matrix $\boldsymbol{F}'$:

$$\boldsymbol{F}' = \begin{bmatrix} \boldsymbol{F} + \boldsymbol{R}\boldsymbol{S} & \boldsymbol{R} \\ \boldsymbol{S} & \boldsymbol{I}_M \end{bmatrix},$$

where $\boldsymbol{I}_M$ is the size-M identity matrix and $\boldsymbol{S}, \boldsymbol{R}$ enforce parity-check relations between the N CW bits and the M auxiliary bits $\boldsymbol{q}$. These are carefully chosen to reduce the amount of short cycles in the resulting Tanner graph: All girth-4 cycles between 2 successive columns in $\boldsymbol{F}$ can be removed if $\boldsymbol{S}[i, -] = \circlearrowleft_i([1, 1, 0, \ldots, 0])$ and $\boldsymbol{R}[i, j] = \boldsymbol{F}[i, j]\boldsymbol{F}[i, j+1]$. The result is a regular graph structure comprising M connected *kernel* graphs (Fig. 1b), each consisting of two CNs (f_{u_j}, f_{d_j}) and one VN (g_j) corresponding to the $(j+1)^{\textbf{th}}$ auxiliary bit. CN f_{d_j} is connected to the set of CW bit VNs being part of a girth-4 cycle between columns $(j, j+1)$ in $\boldsymbol{F}$. CN f_{u_j} is connected to the remaining set of CW bit VNs and the auxiliary bit VN of the previous kernel graph $j-1$.

D. Turning the CSF Matrix into an MBC Structure

CSF matrix $\boldsymbol{F}$ can be decomposed into two sub-matrices: $K \times M$ sub-matrix $\boldsymbol{F}_x$ consists of the first K rows of $\boldsymbol{F}$ related to the systematic bits ($\boldsymbol{x}$), while sub-matrix $\boldsymbol{F}_z$ consists of the subsequent M rows, related to the parity bits ($\boldsymbol{z}$): $\boldsymbol{F} = [\boldsymbol{F}_x \mid \boldsymbol{F}_z]$, $\mid$ indicating row-concatenation. Due to the construction of $\boldsymbol{F}$ from circularly shifted sequences $\boldsymbol{x}_i^{\perp}$ of period r, submatrices $\boldsymbol{F}_x$ and $\boldsymbol{F}_z$ exhibit inherent periodic structure. In particular, $\circlearrowleft_{\omega-1}(\boldsymbol{F}_z)$ forms a circulant matrix generated by a length-ω polynomial $\boldsymbol{T}_z$. Furthermore, each block of r rows in $\boldsymbol{F}_x$ is a column-wise circular shift of the preceding block and contains an identical non-zero sub-block $\boldsymbol{T}_x$ of size $r \times \omega$:

$$\boldsymbol{F}_x[\boldsymbol{k} + ir, -] = \underset{i-\omega+1}{\circlearrowleft}([\boldsymbol{T}_x, \mathbf{0}]), i \in [\![0, M-1]\!], \quad (8)$$

with $\boldsymbol{k} = [0, \ldots, r-1]$. The polynomial $\boldsymbol{T}_z$ and sub-block $\boldsymbol{T}_x$ can then be combined into a unified structure, referred to as the linear transformation block (LTB), defined as $\boldsymbol{T} = [\boldsymbol{T}_x \mid \boldsymbol{T}_z]$. This LTB enables the successive computation of syndrome bits at each time index j. In particular, the input vectors $\boldsymbol{x}_j$ and $\boldsymbol{z}_j$, of dimensions r and 1 respectively, are extracted from the punctured CW $\tilde{\boldsymbol{c}} = [\boldsymbol{x}, \boldsymbol{z}]$ such that

$$\boldsymbol{x}_j = \boldsymbol{x}[\boldsymbol{k} + jr], \boldsymbol{z}_j = \boldsymbol{z}[j], \forall j \in [\![0, M-1]\!]. \quad (9)$$

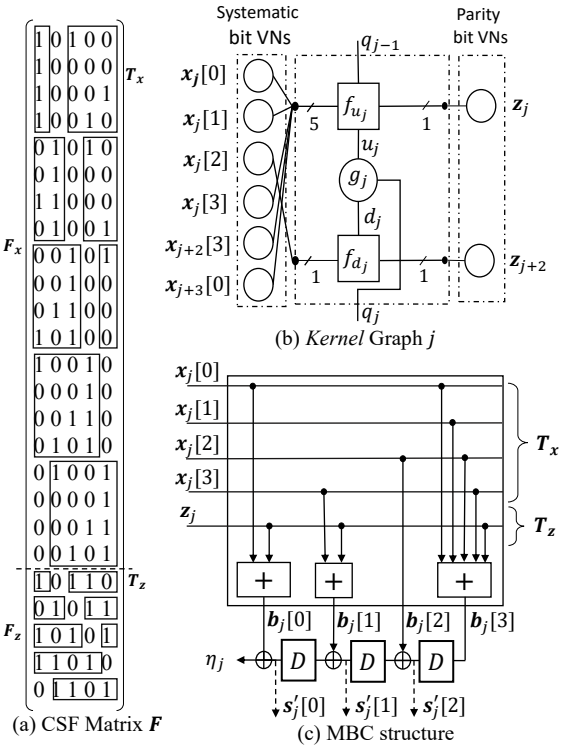

(a) CSF Matrix $\boldsymbol{F}$ (b) *Kernel* Graph j (c) MBC structure

Figure 1. Example of a rate $R = r/(r+1)$ code with regular puncturing: (a) CSF matrix for the TB-RSC code with $\boldsymbol{g}_r = [1, 1, 0, 1] = (15)_8$ and $\boldsymbol{g}_p = [1, 0, 1, 1] = (13)_8$, with $K = 20$, punctured to $R = 4/5$ via $\boldsymbol{m} = [0, 4, 8, 12, 16]$. (b) One base graph among $M = 5$ within the PCM. (c) Corresponding MBC structure.

Then, the input vectors $\boldsymbol{x}_j$ and $\boldsymbol{z}_j$ generate an intermediate output $\boldsymbol{b}_j$ via the transformation matrix $\boldsymbol{T}$ as

$$\boldsymbol{b}_j = [\boldsymbol{x}_j, \boldsymbol{z}_j] \times \boldsymbol{T}, \quad \forall j \in [\![0, M-1]\!]. \quad (10)$$

To compute the full syndrome vector $\tilde{\boldsymbol{c}}\boldsymbol{F}$, outputs from the previous $\omega - 1$ time steps, i.e., $\boldsymbol{b}_{j-v}$ for $v \in [\![1, \omega-1]\!]$, must be taken into account. The aggregated contribution at time j yields the syndrome bit η_j, given by

$$\eta_j = \bigoplus_{v=0}^{\omega-1} \boldsymbol{b}_{j-v}[v]. \quad (11)$$

To enable efficient data reuse, the expression in (11) can be implemented using a feed-forward convolutional architecture with $\nu' = \omega - 1$ MEs. The output vector $\boldsymbol{b}_j$ is used to update the MEs $\boldsymbol{s}'_j$, which are initialized based on the tail-biting circular state and updated for all $j \geq 0$ as

$$[\eta_j, \boldsymbol{s}'_j] = [\boldsymbol{s}'_{j-1}, 0] + \boldsymbol{b}_j. \quad (12)$$

The resulting scheme corresponds to the MBC structure illustrated in Fig. 1c, where inputs $\boldsymbol{x}_j$ and $\boldsymbol{z}_j$ are processed by $\boldsymbol{T}$ to compute the updated state $\boldsymbol{s}'_j$ and generate output η_j. For a valid CW $\boldsymbol{c}$, output η_j satisfies $\eta_j = 0$ for all $0 \leq j < M$.

IV. Decoding using the CSF Matrix

The MBC structure derived from the proposed CSF matrix can be directly decoded using the max-log-MAP (MLM) algorithm [7] by building its trellis representation [8]. Forward and backward recursions, along with branch metrics (α, β, and γ), are computed on a radix-2^r trellis with $2^{\nu'}$ states and 2^r transitions per state. To reduce complexity in soft-output (SO) computations over this high-radix trellis, the local-soft output Viterbi algorithm (L-SOVA) algorithm is employed [9].

As an alternative, we can apply BP decoding to the graph structure introduced in Section III-C, using a layered schedule and the min-sum (MS) approximation [10] with an offset of 0.3. Each BP iteration consists of layered message updates in the forward direction (i.e., kernel graph $j \to j+1$), followed by backward updates (kernel graph $j+1 \to j$).

A. Simulation Results

Figure 2 compares the FER and BER performance of the proposed trellis-based and graph-based CSF decoding methods for various code rates, assuming binary phase-shift keying (BPSK) modulation over an additive white Gaussian noise (AWGN) channel. For each rate $R_r, r \neq p$, we set $\boldsymbol{x}^{\perp} = [1, \mathbf{0}_{2r-1}, 1, \mathbf{0}_{r-1}, 1, 0, \dots]$ such that $\boldsymbol{T}_z$ is generated by the polynomial $[1, 1, 0, 1]$, and $\boldsymbol{x}^{\perp} = [1, \mathbf{0}_{p-1}, 1, 0, \dots]$ if $r = p$, p being the period of $\boldsymbol{g}_r$, $(p = 2^{\nu'} - 1)$. Note that the MLM decoder applied to the MBC structure yields identical SO values as the conventional decoder for punctured CCs. Despite the presence of residual short cycles in the PCM, the MLM decoding across all evaluated code rates with only $\text{it}_{\text{BP}} = 2$ iterations (i.e. only one exchange is needed, backward-forward schedule).

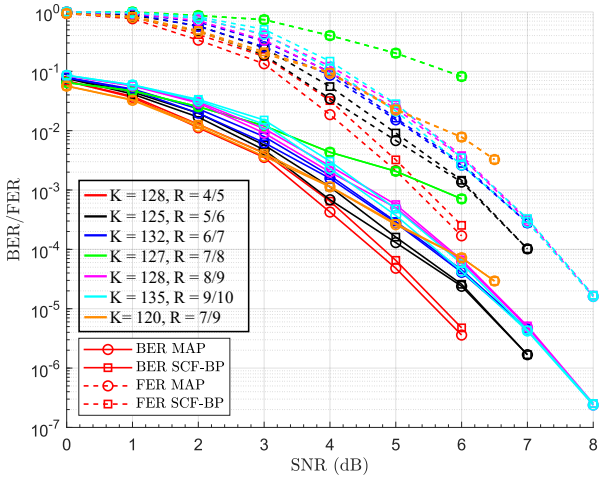

Figure 2. BER and FER Performance Comparison of MLM and BP Decoding.

B. Complexity Assessment

MAP decoding: Considering a regularly punctured CC with rate R_r, if r is not a multiple of the period of $\boldsymbol{g}_r$, the radix-2^r MLM decoder generates r soft outputs (SOs) per trellis stage, each stage comprising $2^{\nu'}$ states and 2^r transitions. In the particular case where the coding rate is $R_p = p/(p+1)$, a two-state trellis can be derived from the CSF matrix, significantly reducing decoding complexity.

Table I
Arithmetic Complexity and Comparison of BP vs. MLM. †: Complexity (Additions , Comparisons), ‡: MLM, *: BP, ♯: % reduction of BP vs. MLM.

Proc.	Complexity†	R_r	d_v,d_c	BP†	MLM†	Red.♯
$\gamma^{\ddagger}$	2^{r-1} , 0	4/5	3, 9	18 , 23	44 , 36	**59, 36**
$\alpha^{\ddagger}$	$2^{\nu'}/r, (2^r - 2^{\nu'})/r$	5/6	3, 10	17, 20	52 , 42	**67, 52**
$\beta^{\ddagger}$	$2^{\nu'}/r, (2^r - 2^{\nu'})/r$	6/7	3, 12	16 , 22	67 , 51	**76, 56**
SO‡	$4 \cdot 2^{\nu'}$, $4 \cdot 2^{\nu'}$	7/8	3, 7	16 , 10	72 , 44	**78, 77**
CN*	$0, 2\text{it}_{\text{BP}}(3d_c - 4)/r$	8/9	3, 16	15 , 22	162 , 94	**90, 76**
VN*	$2\text{it}_{\text{BP}}(d_v + \frac{2d_v}{r})$, 0	9/10	3, 16	15 , 20	290 , 144	**95, 86**

BP decoding: The complexity of the BP decoder is governed by the node degrees d_v and d_c, which are uniform across all kernel graphs in our design. A CN update involves a d_c-to-2 minimum operation, implemented using a sorter of size d_c, resulting in approximately $(3d_c/2 - 2)$ comparisons per output. VN updates require d_v additions. For iterative decoding, this complexity scales linearly with the maximum number of iterations.

Table I summarizes the analytical expressions and numerical values of the arithmetic complexity for various configurations, comparing BP with $\text{it}_{\text{BP}} = 2$ against conventional radix-2^r MLM, normalized by the number of generated SOs. Significant complexity reductions are observed across all code rates when using BP instead of MLM, with minimal performance degradation. Notably, the number of additions and comparisons is reduced by over 50% for all rates, and by more than 90% for $R_9 = 9/10$.

V. Application to Concatenated Codes

A. Decomposition of Convolutional Decoders

The proposed CSF framework enables the decomposition of a rate-$p/(p+k)$ code into k codes, each with rate $p/(p+1)$, thereby facilitating reduced-complexity decoding. This is achieved by splitting the puncturing mask $\boldsymbol{m}$ into k sub-masks $\boldsymbol{m}_j$, with each sub-mask associated with its own CSF matrix. The lower-rate code can then be decoded using k decoders, where the j^{th} decoder takes as input the *a priori* information on the systematic vector $\boldsymbol{x}$, the parity bits given by $\boldsymbol{m}_j$ and iteratively exchanges extrinsic information on $\boldsymbol{x}$ with the other $k-1$ decoders.

As a proof of concept, consider a rate-1/2 CC with $K = 120$ punctured to $R = 7/9$ via the mask $\boldsymbol{m}$, split into two sub-masks $\boldsymbol{m}_1$ and $\boldsymbol{m}_2$[4], yielding two rate-$7/8$ CSF matrices, $\boldsymbol{F}_1$ and $\boldsymbol{F}_2$. The resulting BER/FER performance under BPSK modulation over an AWGN channel with $\text{it}_{\text{BP}} = 2$ is shown in Fig. 2 (orange curves). MLM decoding on the MBC trellis and BP decoding on the cycle-free CSF PCMs, using the MS approximation [10], exhibit identical performance, as the absence of cycles in the PCMs ensures the matching of SOs.

[4] $\boldsymbol{m} = [\boldsymbol{m}_1, \boldsymbol{m}_2]$, with $\boldsymbol{m}_1[j] = 7j$ and $\boldsymbol{m}_2[j] = 7j + 3$

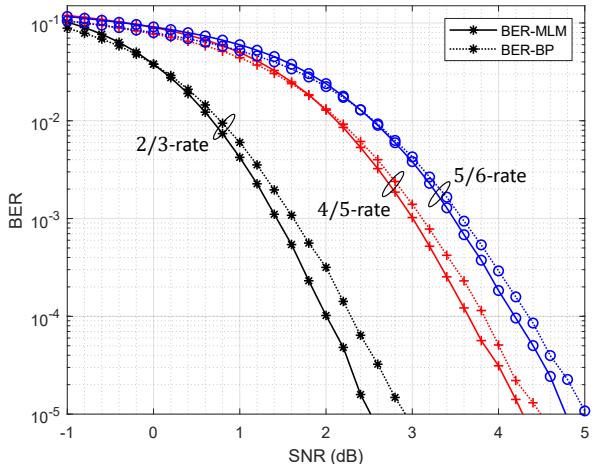

Figure 3. Performance of TC Decoding using BP on CSF.

In terms of complexity, the decomposed decoding of the rate-$7/9$ CC requires 32 additions and 20 comparisons per SO for both of the two rate-$7/8$ decoders, versus 80 additions and 44 comparisons for MLM decoding of the original rate-$7/9$ CC. This yields a 60% reduction in additions and 54% in comparisons.

B. Turbo Decoding using BP on the CSF matrix

For rate$-r/(r+2)$ TCs [11], each constituent CC operates at rate R_r and can be decoded using BP on the CSF PCM (Section III-B) to reduce complexity. As turbo decoders consist of two component decoders connected via an interleaver/de-interleaver[5], the overall complexity reduction for both decoding approaches aligns with the results in Table I.

Figure 3 shows the BER performance under BPSK modulation over an AWGN channel with 8 turbo iterations, for $K = 128$ and code rates $2/3$ and $4/5$, as well as $K = 120$ with rate $5/6$. An extrinsic scaling factor of 0.75 and an offset of 0.3 are respectively used for MLM and MS. The proposed BP-based decoding on the CSF PCM incurs a performance loss of 0.3 dB at BER $= 10^{-4}$ for rate $2/3$. However, at higher rates, the degradation decreases to reach as low as 0.15 dB for rate $5/6$ compared to MLM.

In this final scenario, the decoding complexity is reduced to less than one-tenth of that of the MLM decoder. Furthermore, for lower rates, additional performance improvements can be achieved by mitigating short cycles in the CSF matrix. These substantial complexity savings pave the way for more advanced performance-enhancing techniques, such as multiple-bases BP decoding [13].

VI. Conclusion

This work introduces an alternative representation of CCs that simplifies their decoding process, specifically targeting regularly punctured codes of rate $r/(r+1)$. The proposed approach leverages a novel CSF matrix, derived from a reformulation of the parity constraints between information and redundancy bits. This matrix serves as the foundation for constructing either a MBC structure or a Tanner graph. The MBC representation enables efficient decoding using the MAP algorithm or its approximations on the MBC trellis, while the graph allows for BP decoding. For high coding rates, BP-based decoding on the graph derived from the CSF matrix achieves up to **90%** complexity reduction compared to conventional MLM decoding, with a marginal performance loss of 0.1 dB.

Additionally, we propose a decoding decomposition method for low-rate CCs into multiple iterative decoders operating on higher-rate components. This technique maintains performance while enabling further reductions in decoding complexity. Finally, applying the proposed framework to turbo decoding confirms similar complexity benefits with negligible performance degradation at higher rates.

[5]For Fig. 3, we use almost regular permutation (ARP) interleavers [12]: $\Pi(i) = \mathrm{mod}_K\big(P \cdot i + \boldsymbol{S}[\mathrm{mod}_Q(i)]\big)$, with $P = 79$, $Q = 8$, $\boldsymbol{S} = [14, 105, 123, 111, 83, 87, 83, 42]$ for $K = 128$ and $P = 77$, $Q = 4$, $\boldsymbol{S} = [1, 103, 89, 107]$ for $K = 120$.

Acknowledgements

This work was partially funded by the Important Project of Common European Interest on Micro-Electronics and Communications Tech. led by Orange "IPCEI ME/CT Part".

References

[1] Third Generation Partnership Project, *LTE; Evolved Universal Terrestrial Radio Access (E-UTRA); Multiplexing and channel coding (3GPP TS 36.212 version 18.0.0 Release 18)* , Sep. 2023.

[2] S. Weithoffer and N. Wehn, "Where to go from here? new cross layer techniques for lte turbo-code decoding at high code rates," *Advances in Radio Science*, vol. 16, pp. 77–87, 2018. [Online]. Available: https://ars.copernicus.org/articles/16/77/2018/

[3] H. Ma and J. Wolf, "On tail biting convolutional codes," *IEEE Trans. Commun.*, vol. 34, no. 2, pp. 104–111, 1986.

[4] M. Bazzal, J. Nadal, S. Weithoffer, C. Abdel Nour, and C. Douillard, "Efficient decoder-free minimum distance estimation for concatenated convolutional codes," in *IEEE 101st Veh. Technol. Conf. (accepted for publication)*, Oslo, July 2025.

[5] J. Jabour, J. Nadal, S. Weithoffer, C. Abdel Nour, and C. Douillard, "New Perspectives on Convolutional Coding/Decoding for 6G," in *ASILOMAR Conf. on Sig, Syst., and Comput.*, October 2024.

[6] J. S. Yedida, J. Chen, and M. P. C. Fossorier, "Generating code representations suitable for belief propagation decoding," in *Proc. Annu. Allerton Conf. Commun. Control Comput. (Allerton)*, vol. 40, no. 1, 2002, pp. 447–456.

[7] P. Robertson, E. Villebrun, and P. Hoeher, "A comparison of optimal and sub-optimal decoding algorithms in the log domain," in *IEEE Intl. Conf. Commun., Seattle, WA, USA*, Jun. 1995, p. 1009–1013.

[8] A. Viterbi, "Convolutional codes and their performance in communication systems," *IEEE Trans. Commun. Technol.*, vol. 19, no. 5, pp. 751–772, 1971.

[9] V. H. S. Le, C. Abdel Nour, E. Boutillon, and C. Douillard, "Revisiting the Max-Log-Map algorithm with SOVA update rules: new simplifications for high-radix SISO decoders," *IEEE Trans. Commun.*, vol. 68, no. 4, pp. 1991–2004, 2020.

[10] M. Fossorier, M. Mihaljevic, and H. Imai, "Reduced complexity iterative decoding of low-density parity check codes based on belief propagation," *IEEE Trans. Commun.*, vol. 47, no. 5, pp. 673–680, 1999.

[11] C. Berrou and A. Glavieux, "Near optimum error correcting coding and decoding: turbo-codes," *IEEE Trans. Commun.*, vol. 44, no. 10, pp. 1261–1271, Oct 1996.

[12] R. Garzón-Bohórquez, C. Abdel Nour, and C. Douillard, "Protograph-Based Interleavers for Punctured Turbo Codes," *IEEE Trans. on Commun.*, vol. 66, no. 5, pp. 1833–1844, Dec. 2018.

[13] T. Hehn, J. B. Huber, S. Laendner, and O. Milenkovic, "Multiple-bases belief-propagation for decoding of short block codes," in *2007 IEEE Intl. Symp. Info. Theory*, 2007, pp. 311–315.